Low-Stiffness Silicon Cantilevers with Integrated Heaters and Piezoresistive Sensors for High-Density AFM Thermomechanical Data Storage

Benjamin W. Chui, *Student Member, IEEE,* Timothy D. Stowe, Yongho Sungtaek Ju, Kenneth E. Goodson, Thomas W. Kenny, H. Jonathon Mamin, Bruce D. Terris, Robert P. Ried, *Member, IEEE,* and Daniel Rugar, *Member, IEEE*

***Abstract*— Single-crystal silicon cantilevers 1 μm thick have been demonstrated for use in high-density atomic-force microscopy (AFM) thermomechanical data storage. Cantilevers with integrated piezoresistive sensors were fabricated with measured sensitivities $\Delta R/R$ up to 7.5×10^{-7} per Å in close agreement with theoretical predictions. Separate cantilevers with integrated resistive heaters were fabricated using the same basic process. Electrical and thermal measurements on these heating devices produced results consistent with ANSYS simulations. Geometric variants of the cantilever were also tested in order to study the dependence of the thermal time constant on device parameters. Depending on the design, time constants as low as 1 μs were achieved. A thermodynamic model was developed based on the cantilevers geometry and material properties, and the model was shown to predict device behavior accurately. A comprehensive understanding of cantilever functionality enabled us to optimize the cantilever for high-speed thermomechanical recording. [264]**

I. Introduction

MICROMACHINED cantilevers have been widely used in atomic-force microscopy (AFM) for imaging purposes [1]–[3]. Alternate uses have also been explored, for example in nanolithography [4]–[6] and high-density data storage [7]–[10]. This paper describes recent developments in one AFM-based recording technique in particular, that of thermomechanical data storage [11], with a focus on the integration of heating and deflection-sensing elements onto the micromachined cantilevers.

In AFM thermomechanical data storage, digital information is represented as submicron data pits on a rotating substrate. In a typical implementation, the sharp tip of a cantilever is kept in continuous contact with a spinning polycarbonate disk by a weak loading force on the order of 10^{-7} N. For writing, the cantilever tip is heated above the glass transition temperature of polycarbonate (which is approximately 120 °C) while subjected to the loading force, thereby melting data pits onto the substrate. For reading, the cantilever deflection is measured as the tip rides over the pits. Bit densities up to 30 Gb/in^2 (50 times CD-ROM) have been demonstrated [12]. With low-mass cantilevers, readback rates up to 1.2 Mb/s have been achieved [12].

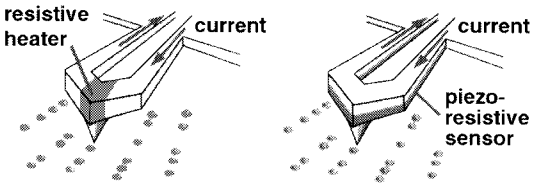

Fig. 1. Principle of thermomechanical data storage using (a) cantilevers with built-in heaters for writing and (b) integrated piezoresistive sensors for readback.

Originally, writing was achieved by heating the tip with a laser beam, and reading was achieved by measuring the deflection of a second laser beam off the cantilever. A major disadvantage of this method is that the lasers are bulky and require precise alignment. While some simplification has been obtained using a tapered optical fiber as a cantilever [13], the ultimate goal is to develop cantilevers with integrated reading or writing elements that do not rely on lasers, as shown in Fig. 1. For this purpose, we have developed single-crystal silicon cantilevers with piezoresistive elements for readback, based on the approach of Tortonese *et al.* [14]–[16]. We have also made separate cantilevers with integrated resistive heaters for writing [17], [18].

The ideal integrated cantilever will have to satisfy many conditions simultaneously. In order to read marks at densities of 20–50 Gb/in^2, it must have a tip with a radius of curvature below 500 Å. To achieve adequate signal-to-noise ratio, it needs a sensor capable of detecting 10 Å of motion in the readback bandwidth. The device must be soft, with a stiffness of 1 N/m or less, to allow for operation at loads below 10^{-7} N, which is necessary to avoid wear of the tip or sample. At the same time, the resonant frequency should be as high as possible. The combination of low stiffness and high frequency requires the cantilever to have low mass. For writing, an

Manuscript received April 17, 1997; revised October 25, 1997. Subject Editor, K. Petersen. This work was supported by an IBM Cooperative Fellowship, the National Science Foundation CAREER Program (ECS-9 502 046), the National Science Foundation Instrumentation for Materials Research Program (DMR-9 504 099), and the Charles Lee Powell Foundation. The work of H. J. Mamin and R. P. Ried was supported in part by ARPA Contract DABT63-95-C-0019.

B. W. Chui, T. D. Stowe, Y. S. Ju, K. E. Goodson, and T. W. Kenny are with the Departments of Electrical Engineering and Mechanical Engineering, Stanford University, Stanford, CA 94305-4021 USA.

H. J. Mamin, B. D. Terris, R. P. Ried, and D. Rugar are with IBM Research Division, Almaden Research Center, San Jose, CA 95120-6099 USA.

Publisher Item Identifier S 1057-7157(98)02038-1.

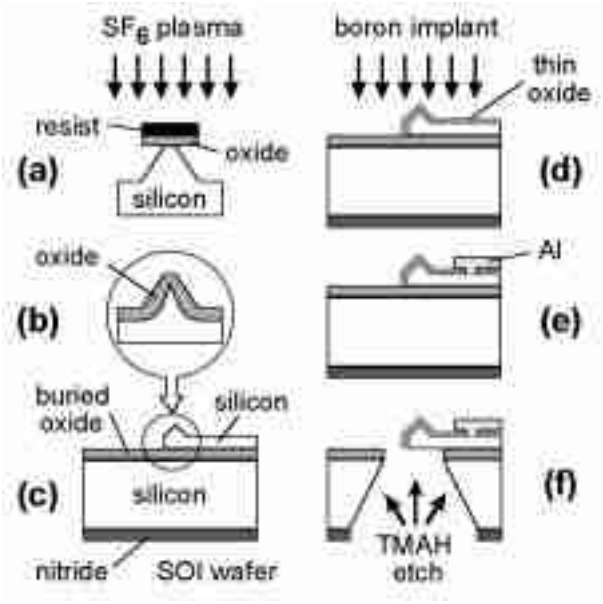

Fig. 2. Fabrication process for 1-μm-thick cantilevers.

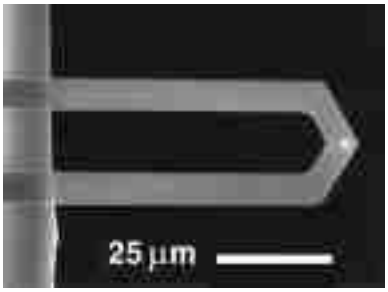

(a)

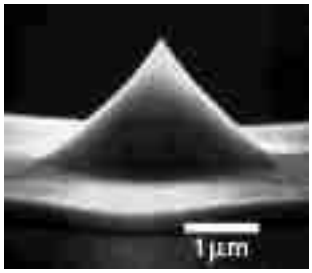

(b)

Fig. 3. Scanning electron microscope images of (a) released cantilever and (b) tip.

integrated element for heating the tip is required, and the thermal time constant should be as short as possible, preferably on the order of 1 μs.

In this work, we have focused on two areas in particular. First, we have integrated piezoresistive sensors with cantilevers that are at least two times thinner than previous devices [14]–[16]. With a cantilever of stiffness 1 N/m, we have measured a deflection sensitivity of 0.016 $\text{Å}/\sqrt{\text{Hz}}$ and a calculated resonant frequency of 280 kHz. To achieve this combination, we had to use novel processing techniques involving rapid thermal anneal to make thin cantilevers 1 μm thick with piezoresistors confined to less than half the cantilever thickness. Second, we have fabricated cantilevers with integrated electrical heating elements and have observed thermal time constants as low as 1 μs. We have implemented both types of cantilevers on a rotating sample to demonstrate reading and writing without lasers.

II. Cantilever Fabrication

The fabrication process for the cantilevers, shown in Fig. 2, has been adapted from reference [16]. The starting material is a silicon-on-insulator (SOI) wafer [19] with a 5-μm-top silicon layer. In Fig. 2(a), an SF_6 plasma etch is used to undercut an oxide-resist mask to form a blunt tip, which is then sharpened by low-temperature oxidation [Fig. 2(b)]. In Fig. 2(c), the cantilever itself is patterned and 1000 Å of thermal oxide is grown to form an electrical passivation layer. (Because the oxide layer is thin, the curvature of the finished cantilever due to stress in the oxide layer is insignificant.) After this step, in a departure from [16], which calls for preoxidation implantation, a series of boron implants are performed through the 1000 Å of oxide [Fig. 2(d)]. In the case of the piezoresistive cantilevers, a first boron implant is performed at 40 keV with a dose $5 \times 10^{14}/\text{cm}^2$ to form the piezoresistive layer, and a second boron implant is performed at 40 keV with a dose of $5 \times 10^{15}/\text{cm}^2$ to produce heavily doped ohmic contact regions. (The implant sequence used to make the heaters is slightly different and will be described in the next section.) Instead of a conventional furnace anneal, the implants are activated by a 10-s rapid thermal anneal at 1000 °C in order to minimize boron diffusion. This results in a shallow piezoresistive layer extending 0.4 μm below the cantilever surface [20]. In general, the shallower the piezoresistive layer relative to the overall cantilever thickness, the better the performance of the resulting piezoresistive sensor. A variant of this rapid thermal anneal method has been adopted by Ried *et al.* in producing piezoresistive cantilevers 0.34 μm thick [21]. In Fig. 2(e), contact vias are etched through the oxide, and aluminum is deposited and patterned to form electrical connections to the cantilever. A backside etch in tetramethyl ammonium hydroxide solution is used to remove the bulk silicon underneath the cantilever [Fig. 2(f)]. A low-stress polyimide layer and a one-sided etch setup is used to protect the front side of the wafer during this step. Finally, the polyimide is removed in an oxygen plasma etch to release the cantilevers.

Fig. 3 shows an scanning electron microscope (SEM) micrograph of a fabricated cantilever and a close-up of the tip. The tip is seen to be very sharp, with a radius of curvature below 300 Å. Such a tip should be suitable for reading and writing marks on a 1000-Å scale.

III. Characterization of Piezoresistive Cantilevers

The sensitivity of the piezoresistive cantilevers was measured by placing the cantilever on a piezoelectric actuator (which is part of an AFM) and oscillating the cantilever support with the tip in contact with a fixed surface. Typical oscillation amplitudes were on the order of 1000 Å. The piezoresistive response for a given oscillation amplitude was measured with a simple full bridge circuit based on a

TABLE I
COMPARISON OF PIEZORESISTIVE CANTILEVERS FROM THIS WORK AND TORTONESE *et al.*

	L_1 (μm)	t(μm)	measured ΔR/R per Å	$k^{(a)}$	MDD[(b)]	FFOM[(c)]
This work	75	1	7.5×10^{-7}	1.5	0.5	0.075
Tortonese *et al* [16]	175	2	1.2×10^{-7}	4	1.35	0.54
Tortonese *et al* [15]	170	4	8.5×10^{-7}	16.4	0.2	0.33

[(a)] Calculated spring constant (N/m)
[(b)] Minimum detectable deflection in 10 Hz-1 kHz bandwidth (Å)
[(c)] Force figure of merit (= MDD × k) (nN)

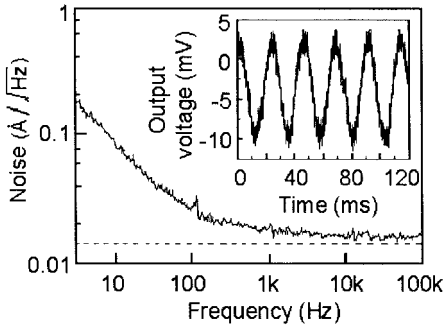

Fig. 4. Noise spectrum of a 75-μm piezoresistive cantilever. The theoretical Johnson noise floor is shown as the dotted line. Inset: cantilever response to 100-Å modulation.

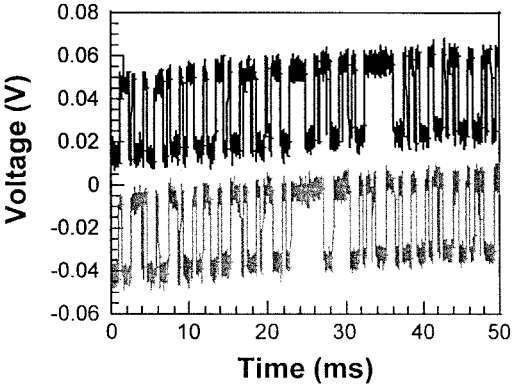

Fig. 5. Readback signals obtained in parallel with two 150-μm piezoresistive cantilevers operated on a spinning test sample with 1100-Å-deep grooves.

Burr–Brown INA103 instrumentation amplifier. This amplifier has an input noise of 1 nV/$\sqrt{\text{Hz}}$ and a gain-bandwidth product of 100 MHz. We operated with a bridge supply voltage of 5 V (i.e., 2.5 V across each resistor) and a gain of 100. Since the cantilever resistance was 5–30 kΩ (depending on length and doping concentration), the power dissipated in the cantilever was 1 mW or less. Measured values of piezoresistive sensitivity obtained for cantilevers of various lengths were in close agreement with theory [16], [17].

For a 75-μm-long cantilever, a piezoresistive sensitivity $\Delta R/R$ of 7.5×10^{-7} per Å was measured. This compares favorably to other piezoresistive sensors, while our device has much lower stiffness. Compared with Tortonese *et al.* [15], [16], our cantilever has a more favorable force figure of merit due to its lower spring constant (Table I).

Fig. 4 shows the noise spectrum of a 75-μm-long cantilever. The observed noise floor of 1.6×10^{-2} Å/$\sqrt{\text{Hz}}$ is very close to the Johnson noise floor of 1.3×10^{-2} Å/$\sqrt{\text{Hz}}$. With its knee around 200 Hz, the integrated $1/f$ noise from 1–200 Hz is only about 0.5 Å. The inset of Fig. 4 shows the response of the cantilever to a 100-Å oscillation applied with the AFM. The measurement bandwidth used in this experiment was 1–100 kHz, within which the minimum detectable displacement was below 10 Å. Since data pits on the polycarbonate disk are typically 100–200 Å deep, piezoresistive readback of real data pits should be possible at this bandwidth.

Fig. 5 shows readback signals obtained simultaneously for a pair of 150-μm-long piezoresistive cantilevers operated in parallel. The cantilevers were operated on a spinning silicon test sample with a rectilinear pattern of 1100-Å-deep grooves. The bandwidth in this case was 30 kHz, and the linear velocity was approximately 20 mm/s. No independent load control was used for the cantilevers. Because of the low stiffness of the cantilevers, however, it was possible to bring both tips into contact with the sample while maintaining acceptably low loading forces, in this case below 5×10^{-8} N. Because these cantilevers were relatively long, the sensitivity and bandwidth were not as high as with the 75-μm cantilever described in Fig. 4. Still, this experiment does show the basic feasibility of parallel piezoresistive readback with a reasonable signal-to-noise ratio on a fast-rotating sample.

It is also desirable to perform similar readback tests with the tip in contact with a polycarbonate sample instead of a silicon sample. Such an environment is more representative of the actual data-storage application and is expected to reduce tip-sample wear. Long-term tip-sample wear characteristics have been studied in greater detail in a separate experiment [22].

IV. CANTILEVERS WITH INTEGRATED HEATERS

In addition to piezoresistive cantilevers, the fabrication process of Fig. 2 has also been used to produce heater-cantilevers by selectively doping different parts of the cantilever. This is possible because the cantilever material is single-crystal silicon, which can be doped to give a wide range of resistivity. This is convenient for electrical heating, as it allows us to make the heating element and the leads of the same material. Single-crystal silicon cantilevers have intrinsically low stress and high thermal conductivity. Other approaches to micromachined heating elements include polysilicon [23] and nickel silicide [24].

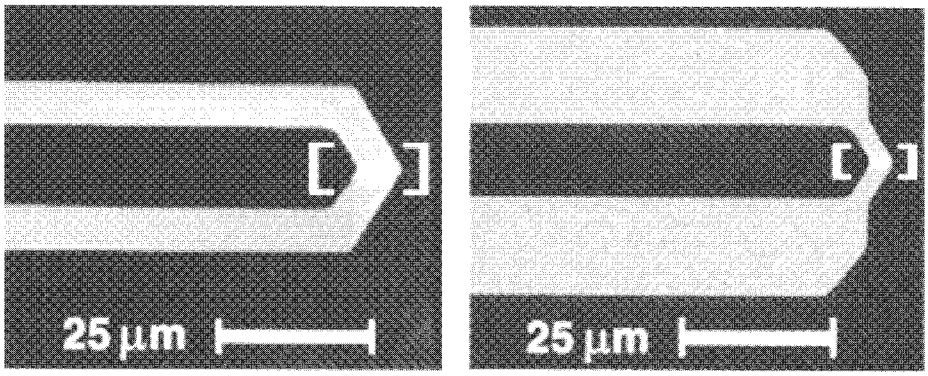

(a) (b)

Fig. 6. Scanning electron microscope images of (a) Type-A boron-doped "nonconstricted" heater and (b) Type-B phosphorus-doped "constricted" heater. In each case, the region enclosed by the brackets represents the lightly doped resistive heater while the rest of the cantilever is heavily doped.

The ion implant sequence used to make the heater-cantilevers is slightly different from that for the piezoresistive cantilevers. First, a low-dosage blanket implant is performed on the entire cantilever and furnace-annealed for an extended amount of time in order to establish an essentially uniform background doping level. After that, the cantilever is subjected to a heavy implant step during which a region around the tip is masked off, and the implant is activated by rapid thermal anneal. The masked region becomes a relatively lightly doped region at the tip of the cantilever—the resistive heater—which is electrically connected to the base via highly conducting legs (see Fig. 6). The actual resistivity of the heater region can be adjusted by changing the dosage of the first blanket implant step. To operate the heater, a current pulse is passed through the cantilever to cause significant power dissipation in the heater region, resulting in a localized temperature rise. After the pulse has passed, the heat is carried away mainly by conduction down the legs to the base.

We have fabricated and tested two types of heater-cantilevers: Type-A heaters [Fig. 6(a)] are boron doped, with a background implant of $8 \times 10^{12}/\text{cm}^2$ and a heavy implant of $5 \times 10^{15}/\text{cm}^2$. Type-B heaters [Fig. 6(b)] are phosphorus doped, with a background implant of $1.5 \times 10^{14}/\text{cm}^2$ and a heavy implant of $10^{16}/\text{cm}^2$. An advantage of Type-A heaters is that it is possible to make piezoresistive cantilevers and heaters on the same die with shared boron implant steps. An advantage of Type-B heaters is that with phosphorus it is possible to dope silicon to higher electrical conductivity, reducing the resistance of the cantilever legs. To improve heating and cooling efficiency, Type-B devices also have shorter, wider legs as well as a heater constriction.

V. Thermal and Electrical Measurements

The thermal characteristics of the heaters can be probed electrically, by using the temperature-dependent resistivity of the heater as an on-board thermometer. This method of measurement has previously been used to characterize micro-lamps [23] as well as commercial AFM cantilevers [25]. With this method, it is first necessary to determine the temperature coefficient of resistance of the heaters. The temperature coefficient of resistance has been measured for a 200-μm-long Type-A cantilever with an 8-μm heater region. The device chip was placed on a temperature-controlled chuck, and an HP4155A semiconductor parametric analyzer was used to apply a 100-mV test voltage across the 9-kΩ cantilever resistance and to measure the resulting current. Measurements indicate positive temperature coefficients of resistance for the legs and the heater region of approximately 0.1% and 0.3%/°C, respectively. One would therefore expect that when a voltage pulse is applied to the cantilever, its resistance would increase as it heats up. This increase in resistance can be measured by monitoring the current through the cantilever. After the pulse has elapsed, the heater resistance would gradually decrease to its room-temperature value as it cools. If a small dc test voltage is present across the cantilever after the pulse has ended, this decrease in resistance can be measured as well. It is therefore possible to measure the temperature of the heater during both the heating stage and the cooling stage. The rate of cooling corresponds to the thermal time constant and determines how fast successive marks can be written, i.e., the data writing speed.

In one experiment, an 11-V 5-μs heating pulse [Fig. 7(a)] was applied across the Type-A heater. The instantaneous current through the cantilever was determined from the voltage across a 100-Ω series resistor, and the oscilloscope trace is reproduced in Fig. 7(b). Knowing the voltage and current, the heater resistance can be calculated at every point in time. Because the cantilever legs have a much greater thermal mass than the heater region, its temperature excursions are small in comparison, and therefore changes in its electrical resistance introduce only a slight error into the calculations, below 5% in this case.

To be able to continue monitoring the heater resistance after the voltage pulse has elapsed, a constant 1-V dc offset was applied. The value of 1 V was chosen to avoid significant self-heating. The calculated heater resistance during and after the heating pulse was converted to a temperature scale based on the heater's previously measured temperature coefficient of resistance. The derived heater temperature is shown in Fig. 7(c). It is seen the heating pulse caused the heater temperature to rise to approximately 200 °C [Fig. 7(c), solid line]. Afterwards, the heater cooled toward room temperature

TABLE II
ANSYS FINITE-ELEMENT ANALYSIS PARAMETERS. NOTE THE USE OF TEMPERATURE-DEPENDENT MATERIAL PROPERTIES (THERMAL CONDUCTIVITY, SPECIFIC HEAT, AND ELECTRICAL RESISTIVITY)

	Type A Heaters						Type B Heaters					
	Heavily doped legs			Lightly doped heater			Heavily doped legs			Lightly doped heater		
Temperature (K)	300	400	600	300	400	600	300	400	600	300	400	600
Thermal conductivity (W/m.K)	52	34	22	112	76	50	106	74	46	127	89	55
Specific heat (J/kg.K)	712	790	867	712	790	867	712	790	867	712	790	867
Electrical resistivity ($\mu\Omega$.m)	94	108	140	3200	4750	6500	24	30	41	265	320	428
Density (kg/m^3)	2330			2330			2330			2330		
Mesh size	Ranges from 1 μm (around heater region) to 8 μm (near cantilever base)						Ranges from 1 μm (around heater region) to 8 μm (near cantilever base)					
Time steps	0.02 μs (from t = 0 μs to 10 μs) 0.05 μs (from t = 10 μs to 20 μs) 0.2 μs (from t = 20 μs to 50 μs) 0.5 μs (from t = 50 μs to 100 μs)						0.005 μs (from t = 0 μs to 0.5 μs) 0.01 μs (from t = 0.5 μs to 1 μs) 0.025 μs (from t = 1 μs to 2.5 μs) 0.05 μs (from t = 2.5 μs to 5 μs)					

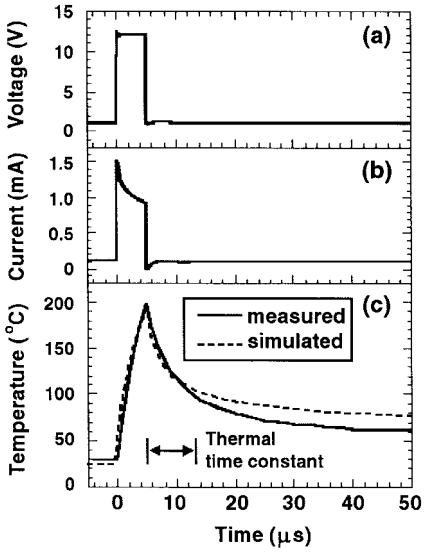

Fig. 7. Electrical measurements for estimating Type-A heater temperature during and after a heating pulse. (a) Applied voltage pulse (amplitude is 12 V at time 0–5 μs and 1 V at all other times). (b) Measured current using a 100-Ω sense resistor. (c) Derived heater temperature showing a thermal time constant of approximately 10 μs.

with a thermal time constant of about 10 μs, compared with 350–450 μs for a commercial silicon cantilever without a localized heater [25].

The thermal time constant of Type-B heaters was measured using a similar electrical method. In this case, a 10-V 0.2-μs pulse was applied, and the result is shown in Fig. 8. It is seen that the time constant for a 100-μm-long cantilever is approximately 0.8 μs, one order of magnitude better than for Type-A heaters. This is due to several reasons. First, the Type-B geometry has shorter, wider legs, which form a better thermal connection between the heater region and the base. Second, the legs are phosphorus doped to higher conductivity, allowing electrical power to be delivered more efficiently to the heater and shorter heating pulses to be used. A shorter heating pulse allows less time for the heat to diffuse from the heater region to the surrounding silicon. The total heat-affected volume is reduced and therefore easier to cool. Third, the heater is now located in a constriction, which has a smaller thermal mass that can be heated and cooled more efficiently.

VI. FINITE-ELEMENT ANALYSIS

Finite-element analysis with ANSYS software was performed to corroborate the experimental measurements on the Type-A and Type-B heaters. The cantilever was represented by a thermal/electrical finite-element model. Standard values of silicon thermophysical properties [26] were used except for thermal conductivity values, which were adjusted down to reflect an experimentally observed reduction due to heavy doping [27], [28], especially in thin silicon films [29]. (Attempts are being made to understand this phenomenon more fully [30].) The variation of thermal conductivity and heat capacity with temperature was represented by a temperature-dependent property table in ANSYS. Two different sets of material properties were defined, one for the heavily doped cantilever legs and another for the more lightly doped heater region.

To reduce simulation time without sacrificing accuracy, a variable mesh size was used for the finite-element model, with the mesh being finest around the heater region where the temperature gradient was expected to be steepest. Variable time steps were also used to reduce simulation time. The smallest time steps were used at the beginning of the simulation period, when the temperature was expected to be changing most rapidly due to the heating pulse. The simulation parameters are listed in Table II.

The actual ANSYS simulation was performed as a transient analysis in which a voltage pulse was applied to the finite-element model, and the temperature rise at the heater region was calculated at specified time intervals. The simulated results, shown by the dotted line in Fig. 7(c) (for the Type-A heater) and Fig. 8 (for the Type-B heater), agree closely with experiment.

VII. LASER THERMOMETRY AND VIBROMETRY MEASUREMENTS

A supplementary type of measurement laser thermometry was used to corroborate the electrical measurements of the

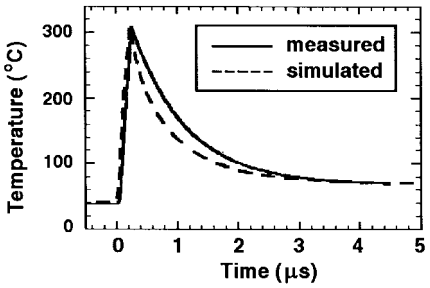

Fig. 8. Time-domain temperature variation of Type-B heater subjected to single heating pulse. The measured thermal time constant is approximately 0.8 μs, representing an order-of-magnitude improvement over Type-A heaters. The dotted line shows finite-element simulation data obtained with ANSYS.

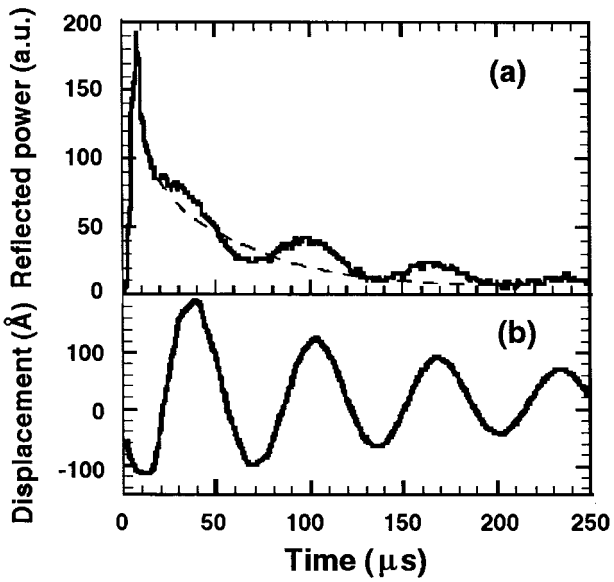

Fig. 9. (a) Reflected laser power from Type-A heater subjected to heating pulse: the dotted line represents the estimated reflectivity curve without mechanical vibration. (b) Laser vibrometer output signal showing mechanical vibration of cantilever tip.

heaters' thermal behavior. Laser thermometry relies on the fact that the optical reflectance of most materials varies with temperature. While this type of measurement is commonly used with metals with up to picosecond-level resolution, in some cases it has been adapted for investigating semiconductor devices [31] such as SOI power transistors [32]. In our experimental setup, a low-power laser beam is focused on a heater-cantilever, and the reflected power is measured at different points in time. The results are used to estimate the heater temperature and the thermal time constant.

Fig. 9 shows the reflected laser power from a location near the tip of a 200-μm-long Type-A cantilever in response to a heating pulse. This curve shows two distinct phenomena: an oscillation at 14 kHz and a decay time on the order of 10 μs. The overall decay is believed to be related to the cantilever's temperature coefficient of reflectivity; the time constant for this decay is consistent with the electrical resistance measurements. In addition, the oscillation is believed to be due to a thermally induced vibration. Since the cantilever has a 1000-Å oxide layer, it is expected to show differential thermal expansion when heated.

To confirm this hypothesis, we used a laser vibrometer [33] to study the pure mechanical behavior of a cantilever in response to a heating pulse. In this technique, a laser interferometer is used to measure the motion of the cantilever tip with angstrom-level resolution. The output of the vibrometer is shown in Fig. 9. A decaying sinusoidal oscillation is observed, confirming the mechanical origins of the oscillation in Fig. 9. From Fig. 9(b), the initial amplitude of the vibration is estimated at 300 Å. It should be pointed out that our measurement of heat-induced mechanical oscillation in the cantilevers does not imply a limitation to their use in data storage. In operation, the cantilevers are placed in continuous contact with the polycarbonate substrate, and the heat pulses do not cause sufficient mechanical oscillation for loss of contact to occur.

As supplementary techniques to electrical measurements, laser thermometry and vibrometry make it possible to characterize cantilever behavior in detail. Laser thermometry can provide spatially and temporally resolved measurements of cantilever temperature; laser vibrometry can do the same for cantilever motion. These two types of measurement will be useful for developing improved cantilevers for thermomechanical data storage and other applications.

VIII. Frequency-Domain Thermal Analysis

The time-domain electrical resistance measurements described above revealed only one of the characteristic time constants of the cantilever. It is possible that longer secondary time constants exist that were not readily observable due to the short time scales used in the measurements. To further understand the relationship between thermal time constants and cantilever geometry, a frequency-domain measurement of a Type-B heater was performed.

In this thermal analysis, a 1.5-V dc signal with a 0.1-V ac component was applied across a Type-B cantilever. An HP 89410 vector analyzer was used to measure the input voltage and the current through the heater (via a series sensing resistor) and to calculate the resulting resistance in real time. This resistance is expected to vary at the same frequency as the ac component of the applied voltage, since the electrical power supply to the heater varies at that frequency. The variation in the resistance of the heater is therefore an indication of its thermal fluctuation. By repeating the measurement at various frequencies between 100 Hz to 1 MHz, a thermal response profile can be obtained for the heater.

Certain general predictions can be made about the frequency response. When the frequency of the ac component is low, the heater temperature is expected to be able to fully follow the variation in the electrical power supply. This is because the heater region (i.e., the tip of the cantilever) can essentially equilibrate itself with the remainder of the structure (i.e., the constriction, the legs and the base) at every point in time by virtue of heat conduction through the cantilever. At higher frequencies, however, the fluctuation in heater temperature will decrease in amplitude because heat diffusion along the cantilever legs is not rapid enough to allow full thermal equalization between the constriction and the base. At

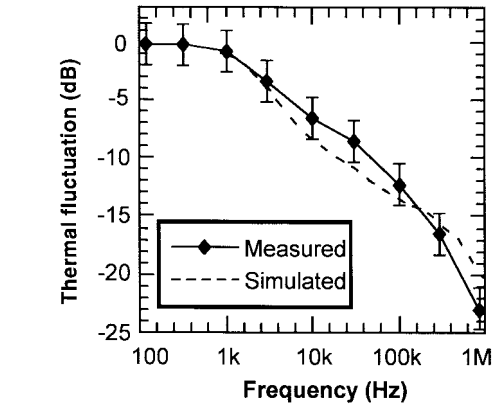

(a)

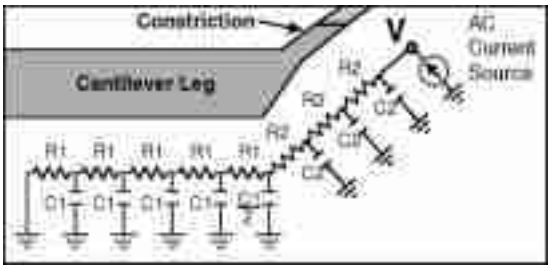

(b)

Fig. 10. (a) Frequency-dependent temperature fluctuation of Type-B heater subjected to sinusoidally varying-input power. The higher the frequency of variation, the smaller the thermal fluctuation. Note the pole at 1 kHz (corresponding to the time constant of the cantilever legs) and a less distinct one around 100 kHz (corresponding to that of the heater constriction). The 0-dB point on the y axis is arbitrary. (b) Capacitor-resistor thermodynamic model based on the cantilever's geometry and material properties. The output signal is measured at point V. Component values: $R1 = 12\,000$ K/W, $C1 = 0.6$ nJ/K, $R2 = 6000$ K/W, and $C2 = 0.01$ nJ/K.

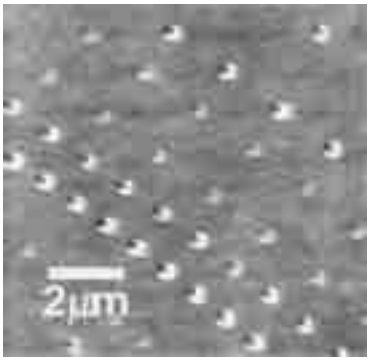

(a)

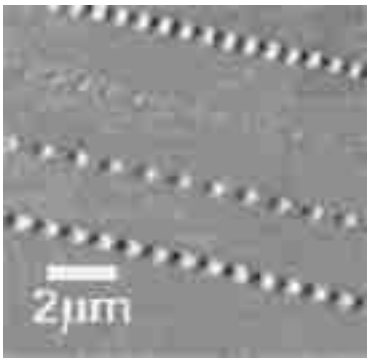

(b)

Fig. 11. Atomic-force microscopy image of sample data tracks written with (a) Type-A heater using 16-V 20-μs pulses with a period of 90–200 μs (about 10 kb/s). (b) Type-B heater using 30-V 0.2-μs pulses with a period of 7–14 μs (about 100 kb/s).

even higher frequencies, the constriction itself cannot support adequate heat exchange between the heater and the legs, so the heater temperature will remain nearly constant.

This prediction is confirmed by the experimental results shown in Fig. 10(a). At low frequencies the temperature fluctuation of the heater is largely constant, but beyond 1 kHz the amplitude of fluctuation decays rapidly with frequency, with an accelerated rate of decay occurring above 100 kHz. Of special interest is the pole on the graph at 1 kHz. This pole corresponds to a "slow" time constant of about 150 μs and is believed to be associated with the cantilever legs. This "slow" time constant was not readily observable from the electrical resistance measurements of Fig. 8.

For calibration purposes, the measurement was also performed on a carbon-film resistor, which undergoes no appreciable heating, and in this case essentially no apparent resistance variation was observed except at frequencies approaching 1 MHz. This variation is believed to be associated with signal distortion in the measurement circuitry rather than the device under test, and the data in Fig. 10 has been adjusted to account for this effect.

To verify the results of the frequency-domain analysis, we analyzed the Type-B heater in SPICE using a thermodynamic model based on the thermal resistances and capacitances of the cantilever. These values were calculated based on the actual dimensions of the cantilever and the thermal conductivity and heat capacity of silicon. The distributed nature of the thermal resistances and capacitances was accounted for by using multiple resistor and capacitor elements to represent each of two sections of the cantilever (the leg and the constriction). The heating element was modeled with an ac current source at the heater tip [see Fig. 10(b)]. Using this model, a simulated frequency response was obtained in good agreement with the measured response. This result shows that it is indeed possible to generate an accurate thermodynamic model for the heater-cantilever based on its dimensions and material properties. This type of thermodynamic modeling will prove useful for designing future devices.

IX. Thermal Writing Experiments

Basic functionality of the heaters have been demonstrated, as shown by the AFM micrograph in Fig. 11. Sample data tracks were written with the heater on a rotating polycarbonate sample. The writing was very reliable, and different-sized marks could be written by varying the pulse conditions. The smallest marks in Fig. 11 correspond to bit densities approaching 10 Gb/in^2, assuming a standard (2,7) code. Since this experiment was aimed at comparing the writing speeds of Type-A and Type-B heaters, the test conditions were not necessarily optimized to produce the maximum bit density.

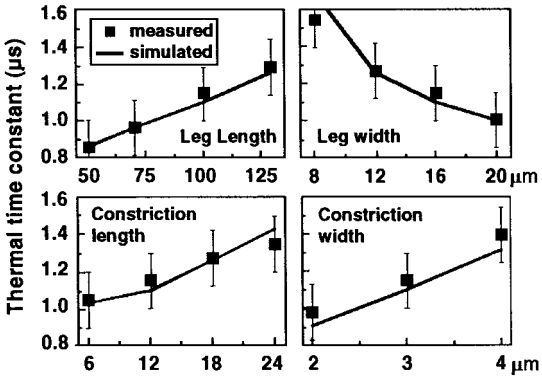

Fig. 12. Measured and simulated thermal time constants for families of Type-B heaters under repeated-pulse conditions. In general, it is seen that shorter wider legs and smaller heater constrictions give rise to shorter time constants. The "nominal" cantilever geometry from which variants are derived [see Fig. 6(b)] has dimensions 100 $\times$ 16 $\times$ 1 μm (for each leg) and 12 $\times$ 3 $\times$ 1 μm (for the constriction).

With Type-A heaters, typical pulse parameters were 16 V and 20 μs with a period of 90–200 μs, implying a writing speed of approximately 10 kb/s. With Type-B heaters, the pulse parameters were 30 V and 0.2 μs with a period of 7–14 μs, implying a writing speed of approximately 100 kb/s, or a tenfold improvement.

X. Heater Design Optimization

In an attempt to find the optimal heater design and to show that the cantilever behavior is understandable and predictable, families of Type-B cantilevers with different geometric configurations were fabricated and tested. Finite-element simulations were also performed for comparison. The measured and simulated thermal time constants are shown in Fig. 12. Cantilever dimensions being varied include the length and width of the cantilever legs as well as the length and width of the heater constriction.

The measurements were performed with repeated heating pulses rather than isolated ones, since the former condition more closely resembles actual operation. In this case, the thermal time constant is expected to differ from the isolated-pulse scenario because the cantilever assumes a pseudosteady-state temperature profile in which the legs experience appreciable heating. For the Type-B cantilever measured earlier, which had a time constant of 0.8 μs under isolated-pulse conditions, it was found that under repeated-pulse conditions the time constant increased slightly to 1.2 μs. This can be attributed to the reduced heat-sinking capability of the legs, which were at an elevated temperature. ANSYS modeling of this scenario confirmed the slight increase in time constant and the elevated temperature profile of the legs.

Measurements on the families of Type-B cantilevers showed, not surprisingly, that the time constant decreases with decreasing constriction length, decreasing leg length, increasing leg width, and decreasing constriction width. The first three trends can be explained by the fact that a smaller thermal resistance from the heater (the cantilever tip) to the heat sink (the cantilever base) is present when the constriction is shorter and the legs are shorter and wider. The last trend is most likely due to the fact that the smaller thermal mass associated with a narrower constriction can be heated and cooled more efficiently—this effect apparently more than offsets the reduced conductivity of the constriction itself.

From the measured data, it is seen that the optimal heater design calls for as short and wide legs as possible and as short and narrow a heater constriction as possible. This rule is obviously subject to practical constraints imposed by fabrication technology, mechanical robustness, and, most importantly, the data-storage system itself. For example, the constriction cannot be made too narrow or the cantilever may break too easily. In addition, the heater region cannot be made too small, in which case its electrical resistance is overwhelmed by that of the legs, making it difficult to deliver power to the heater itself. Most importantly, the cantilever cannot be made too short and too wide, otherwise, its spring constant exceeds the limit for wear-free operation on polycarbonate substrates (approximately 1 N/m in this case).

An effective way of reducing the thermal time constant is to use thinner cantilevers, since this allows shorter and wider legs to be used without increasing the spring constant. For example, given a required spring constant of 1 N/m, a 0.34-μm-thick cantilever can be designed with 40 μm $\times$ 16-μm legs and a 4 μm $\times$ 2-μm constriction. This cantilever is expected to have a thermal time constant below 0.5 μs, according to ANSYS modeling.

XI. Conclusions

In this report, we have described two novel capabilities of AFM cantilevers. First, we have added built-in sensing functionality onto low-stiffness cantilevers with integrated tips. A new process was developed that allows for considerably thinner piezoresistive cantilevers than previously possible, and the process is scalable to even thinner cantilevers. Measured sensitivity is in agreement with predictions, so that we can calculate with confidence the type of cantilever needed to achieve a given level of performance. The current cantilevers are adequate for detecting 100–200-Å-deep features in a 100-kHz bandwidth. They also show excellent $1/f$ noise behavior.

A heater process was developed on separate cantilevers to allow thermal writing without a laser. Thermal time constants as low as 1 μs were achieved with the appropriate cantilever geometry and doping method. Systematic measurement and simulation of different families of cantilevers enabled us to predict an optimized heater design. The accuracy of ANSYS-based finite-element analysis and SPICE simulations was established by virtue of their close agreement with experiment. Furthermore, a thermodynamic model based on the cantilevers material properties proved to be a valuable tool for understanding the thermal behavior of the device. Taken together, these measurement and simulation techniques form a reliable design methodology for future micromachined heaters.

Possibilities for future improvement in AFM thermomechanical data storage include the fabrication of combined read/write devices based on the separately optimized piezoresistive cantilevers and resistive heaters described in this article. Another area of improvement is the use of cantilever arrays

to raise the data throughput. Simultaneous readback with two piezoresistive cantilevers has already been demonstrated, as shown in Fig. 5. Furthermore, the operation of cantilevers in parallel has also been reported in AFM microscopy [34] and nanolithography [35]. One of the advantages of micromachining is that the components are batch fabricated, so that arrays of tips can be easily made. We have been routinely able to fabricate arrays of four cantilevers with high yield, and believe that even larger arrays are possible. Ultimately, parallel operation may prove to be a very effective way of improving the level of performance of AFM thermomechanical data storage.

ACKNOWLEDGMENT

We would like to thank C. F. Quate, S. C. Minne, and H. T. Soh of Stanford for sharing their expertise in AFM cantilever technology and J. D. Plummer of Stanford and L. S. Fan of IBM for their insight on heater behavior. We are also grateful to M. Tortonese of Park Scientific Instruments for helpful discussions and to O. W. Käding for his help with the laser thermometry setup.

REFERENCES

[1] T. R. Albrecht, S. Akamine, T. E. Carver, and C. F. Quate, "Microfabrication of cantilever styli for the atomic force microscope," *J. Vac. Sci. Technol.*, vol. 8, pp. 3386–3396, 1990.
[2] J. Brugger, R. A. Buser, and N. F. de Rooij, "Silicon cantilevers and tips for scanning force microscopy," *Sens. Actuators A*, vol. 34, pp. 193–200, 1992.
[3] O. Wolter, Th. Bayer, and J. Greschner, "Micromachined silicon sensors for scanning force microscopy," *J. Vac. Sci. Technol. B*, vol. 9, pp. 1353–1357, 1991.
[4] A. Majumdar, P. I. Oden, J. P. Carrejo, L. A. Nagahara, J. J. Graham, and J. Alexander, "Nanometer-scale lithography using the atomic force microscope," *Appl. Phys. Lett.*, vol. 6, pp. 2293–2295, 1992.
[5] E. S. Snow and P. M. Campbell, "Fabrication of Si nanostructures with an atomic force microscope," *Appl. Phys. Lett.*, vol. 64, pp. 1932–1934, 1994.
[6] S. C. Minne, H. T. Soh, P. Flueckiger, and C. F. Quate, "Fabrication of 0.1 μm metal oxide semiconductor field-effect transistors with the atomic force microscope," *Appl. Phys. Lett.*, vol. 66, pp. 703–705, 1995.
[7] H. J. Mamin, B. D. Terris, L. S. Fan, S. Hoen, R. C. Barrett, and D. Rugar, "High-density data storage using proximal probe techniques," *IBM J. Res. Develop.*, vol. 39, pp. 681–699, 1995.
[8] R. Barrett and C. F. Quate, "Charge storage in a nitride-oxide-silicon medium by scanning capacitance microscopy," *J. Appl. Phys.*, vol. 70, pp. 2725–2733, 1991.
[9] S. Hosaka, H. Koyanagi, and A. Kikukawa,"Nanometer recording on graphite and Si substrate using an atomic force microscope in air," *Jpn. J. Phys.*, vol. 32, pp. L464–467, 1993.
[10] H. Kado and T. Tohda, "Nanometer-scale recording on chalcogenide films with an atomic force microscope," *Appl. Phys. Lett.*, vol. 66, pp. 2961–2962, 1995.
[11] H. J. Mamin and D. Rugar, "Thermomechanical writing with an atomic force microscope tip," *Appl. Phys. Lett.*, vol. 61, pp. 1003–1005, 1992.
[12] H. J. Mamin, L. S. Fan, S. Hoen, and D. Rugar, "Tip-based data storage using micromechanical cantilevers," *Sens. Actuators A*, vol. 48, pp. 215–219, 1994.
[13] S. Hoen, H. J. Mamin, and D. Rugar, "Thermomechanical data storage using a fiber optic stylus," *Appl. Phys. Lett.*, vol. 64, pp. 267–269, 1994.
[14] M. Tortonese, R. C. Barrett, and C. F. Quate, "Atomic resolution with an atomic force microscope using piezoresistive detection," *Appl. Phys. Lett.*, vol. 62, pp. 834–836, 1993.
[15] M. Tortonese, Ph.D. dissertation, Stanford University, Stanford, CA, 1994.
[16] ——, "Atomic force microscopy using a piezoresistive cantilever," in *Proc. Transducers '91, Int. Conf. Solid-state Sensors and Actuators*, San Francisco, CA, pp. 448–51.
[17] B. W. Chui, H. J. Mamin, B. D. Terris, T. D. Stowe, D. Rugar, and T. W. Kenny, "Low-stiffness silicon cantilevers for thermal writing and piezoresistive readback with the atomic force microscope," *Appl. Phys. Lett.*, vol. 69, pp. 2767–2769, 1996.
[18] B. W. Chui, H. J. Mamin, B. D. Terris, R. P. Ried, D. Rugar, T. D. Stowe, H. T. Soh, S. C. Minne, C. F. Quate, Y. S. Ju, K. E. Goodson, and T. W. Kenny, "Improved cantilevers for AFM thermomechanical data storage," in *Proc. Solid-State Sensor and Actuator Workshop*, Hilton Head, SC, June 2–6, 1996, pp. 219–224.
[19] IBIS Technology Corp., Danvers, MA 01923 USA.
[20] Solecon Laboratories, San Jose, CA 95131 USA.
[21] R. P. Ried, H. J. Mamin, B. D. Terris, L. S. Fan, and D. Rugar, "6-MHz 2-N/m piezoresistive atomic-force-microscope cantilevers with INCISIVE tips," *IEEE J. Microelectromech. Syst.*, vol. 6, no. 4, pp. 294–302, 1997.
[22] B. D. Terris, S. A. Rishton, H. J. Mamin, R. P. Ried, and D. Rugar, "Atomic force microscope based data storage: Track servo and wear study," *Appl. Phys. A*, to be published.
[23] C. H. Mastrangelo, J. H.-J. Yeh, and R. S. Muller, "Electrical and optical characteristics of vacuum-sealed polysilicon microlamps," *IEEE Trans. Electron Devices*, vol. 39, pp. 1363–75, 1992.
[24] J. H. Das and N. C. MacDonald, "Micromachined field emission cathode with an integrated heater," *J. Vac. Sci. Technol. B*, vol. 13, pp. 2432–2435, 1995.
[25] H. J. Mamin, "Thermal writing using a heated atomic force microscope tip," *Appl. Phys. Lett.*, vol. 69, pp. 433–435, 1996.
[26] F. P. Incropera and D. P. de Witt, *Fundamentals of Heat and Mass Transfer*, 3rd ed. New York: Wiley, 1990, Appendix A1.
[27] G. A. Slack, "Thermal conductivity of pure and impure silicon, silicon carbide, and diamond," *J. Appl. Phys.*, vol. 35, pp. 3460–3466, 1964.
[28] L. Weber and E. Gmelin, "Transport properties of silicon," *Appl. Phys. A*, vol. 53, pp. 136–140, 1991.
[29] M. Asheghi, M. N. Touzelbaev, Y. K. Leung, S. S. Wong, and K. E. Goodson, "Temperature-dependent thermal conductivity of single-crystal silicon layers in SOI substrates," *ASME J. Heat Transfer*, vol. 120, pp. 1–7, 1998.
[30] M. Asheghi, B. W. Chui, T. W. Kenny, and K. E. Goodson, "Thermal conduction in single-crystal silicon cantilevers," to be published.
[31] P. W. Epperlein, "Micro-temperature measurements on semiconductor laser mirrors by reflectance modulation: A newly developed technique for laser characterization," *Jpn. J. Appl. Phys.*, vol. 32, pp. 5514–5522, 1993.
[32] Y. S. Ju, O. W. Käding, Y. K. Leung, S. S. Wong, and K. E. Goodson, "Short-timescale thermal mapping of semiconductor devices," *IEEE Electron Device Lett.*, vol. 18, pp. 169–171, 1997.
[33] Polytec Laser Vibrometer OVF-501-0, Polytec P. I., Inc., Costa Mesa, CA.
[34] S. C. Minne, S. R. Manalis, and C. F. Quate, "Parallel atomic force microscopy using cantilevers with integrated piezoresistive sensors and integrated piezoelectric actuators," *Appl. Phys. Lett.*, vol. 67, pp. 3918–3920, 1995.
[35] S. C. Minne, S. R. Manalis, A. Atalar, and C. F. Quate, "Independent parallel lithography using the atomic force microscope," *J. Vac. Technol. B*, vol. 14, pp. 2456–2459, 1996.

Benjamin W. Chui (S'97) received the B.S. and M.S. degrees in electrical engineering from Stanford University, Stanford, CA, in 1992. He is currently working towards the Ph.D. degree at Stanford University.

He worked as an Integrated Circuit Design Engineer for three years. He is currently involved in the fabrication and testing of silicon microcantilevers for AFM thermomechanical data storage in collaboration with the IBM Almaden Research Center and the Stanford Microstructures and Sensors Laboratory.

Mr. Chui received the Henry Ford III Award for highest academic achievement in the school of engineering and is a recipient of the IBM Cooperative Fellowship.

Timothy D. Stowe received the B.S. degree in applied physics from Cornell University, Ithaca, NY, in 1993 and the M.S. degree in applied physics from Stanford University, Stanford, CA, in 1995. He is currently working toward the Ph.D. degree in at Stanford University.

He is currently a John and Fannie Hertz Foundation Fellow at Stanford University. He is a Member of the Stanford Microstructures and Sensors Laboratory and is working in collaboration with the IBM Almaden Research Center on the fabrication and testing of ultrathin cantilevers for nuclear magnetic resonance microscopy.

Yongho Sungtaek Ju received the B.S. degree from Seoul National University, Seoul, Korea in 1993 and the M.S. degree from Stanford University, Stanford, CA in 1995, both in mechanical engineering. He is currently working toward the Ph.D. degree at Stanford University.

He is investigating short-timescale thermal behavior of microdevices and thermal phenomena in nanostructures.

Mr. Ju is a recipient of the University Presidential Award and the Alumni Association Award from Seoul National University.

Kenneth E. Goodson received the B.S., M.S., and Ph.D. degrees in mechanical engineering from the Massachusetts Institute of Technology, Cambridge, in 1989, 1991, and 1993, respectively.

He is an Assistant Professor and Terman Fellow with the Department of Mechanical Engineering, Stanford University, CA. For 16 months starting in 1993, he was with Daimler-Benz AG, Germany, where he worked on the application of CVD diamond layers for the cooling of high-power automotive electronics. He joined Stanford University in 1994, where he now supervises Ph.D. students studying thermal phenomena in electronic micro and nanostructures.

Dr. Goodson's dissertation research on the self-heating of SOI transistors was recognized through the Best Student Paper Award at the 1992 IEEE International Electron Devices Meeting. He is an ONR Young Investigator and a recipient of the NSF CAREER Award.

Thomas W. Kenny received the B.S. degree in physics from the University of Minnesota, Minneapolis, in 1983 and the M.S. and Ph.D. degrees in physics from the University of California, Berkeley, in 1987 and 1989, respectively.

He has worked at the Jet Propulsion Laboratory, where his research focused on the development of electron-tunneling-based high-resolution microsensors. Since 1994, he has been Assistant Professor and Terman Fellow with the Mechanical Engineering Department, Stanford University, Stanford, CA. He currently oversees graduate students in the Stanford Microstructures and Sensors Laboratory, whose research activities cover a variety of areas such as advanced tunneling sensors, small student-built spacecraft, novel fabrication techniques for micromechanical structures, and the study of nonclassical phenomena within this context. In particular, his group is collaborating with researchers from the IBM Almaden Research Center on nuclear magnetic resonance microscopy as well as AFM thermomechanical data storage.

H. Jonathon Mamin received the B.S. degree in physics from Stanford University, Stanford, CA, in 1978 and the Ph.D. degree in physics from the University of California, Berkeley, in 1984.

After receiving the Ph.D. degree, he remained at Berkeley as a Postdoctoral Fellow in the then-emerging field of scanning-tunneling microscopy. Since 1987, he has been a Research Staff Member at the Almaden Research Center, IBM Research Division, San Jose, CA. His research interests include magnetic-force microscopy, surface modification with scanning probes, and high-density data storage.

Dr. Mamin is a Member of the American Physical Society and a Board Member of the Nanometer Scale Science.

Bruce D. Terris received the B.S. degree in applied physics from Columbia University, NY, in 1979 and the M.S. and Ph.D. degrees in physics from the University of Illinois, Urbana-Champaign, in 1981 and 1983, respectively.

After receiving the Ph.D. degree, he was a Postdoctoral Fellow at the Argonne National Laboratory. Since 1985, he has been a research staff member at the Almaden Research Center, IBM Research Division, San Jose, CA. His research interests have included thin-film superconductivity and magnetism, contact electrification of insulators, and new types of scanning-probe microscopes (STM, AFM, near-field optical, etc.). His recent research has focused on the application of proximal probe techniques to high-density data storage.

Dr. Terris is a Member of the American Physical Society.

Robert P. Ried (S'87–M'95) received the B.S. degree from Rice University, Houston, TX, in 1984, the M.Eng. degree from Cornell University, Ithaca, NY, in 1985, and the Ph.D. degree from the University of California, Berkeley, in 1994.

From 1985 to 1987, he was with AT&T Bell Laboratories, Holmdel, NJ, as a Designer of long-distance fiber-optic transmissions systems. He is presently a Postdoctoral Researcher at the Almaden Research Center, IBM Research Division, San Jose, CA. His MEMS research projects have focused on micromachined microphones and scanning-probe data storage.

Daniel Rugar (M'87) received the B.A. degree in physics (*magna cum laude*) from Pomona College, Claremont, CA, in 1975 and the Ph.D. degree in applied physics from Stanford University, Stanford, CA, in 1982.

From 1982 to 1984, he was the Hunt Fellow of the Acoustical Society of America and a Reseach Associate at Stanford University, where he worked on acoustic microscopy and phonon dispersion in superfluid helium. He joined the IBM Research Division, San Jose, CA, in 1984 and has worked on many aspects of high-density data storage and scanning-probe microscopy. His present position is Manager of nanoscale studies. His current research interests include new techniques for ultrahigh-density data storage, magnetic resonance-force microscopy, and ultrasensitive force detection. He has published over 80 papers and holds 13 patents.

Dr. Rugar is a Member of the American Physical Society.